Quantification of Carbon Fibre/Epoxy Resin Composite Failure Processes using Synchrotron Radiation Computed Tomography

H.Morton[1*], P. Reed[1], A, Scott[1], I, Sinclair[1], M. Spearing[1]

[1]*Material's Science Department, University of Southampton*
**h.morton@soton.ac.uk*

Keywords: CFRPs, Failure analysis, SRCT

Abstract

High resolution synchrotron radiation computed tomography (SRCT) has been used to image various carbon/epoxy notched systems as they are incrementally loaded to failure. The high resolution allows the damage mechanisms and the individual micromechanical features to be identified in three dimensions, specifically fibre breaks in this instance. Break densities for different fibre/resin combinations are evaluated and compared, along with variations in break cluster geometry.

1 1ntroduction

Fibre reinforced polymers offer superior properties for structural applications, including high specific stiffness and strength, good fatigue behaviour and excellent corrosion resistance [1]. Many of the reliability issues with composites revolve around the nature and progression of damage [2]; thus an understanding of damage initiation and accumulation under loading is vital for accurate design and life prediction [3]. Without accurate failure models and lifing predictions, design processes must rely on specific, relatively uninformative mechanical tests on large numbers of specimens and prototypes. Whilst there is an established range of composite failure models, including those by Zweben [4], Batdorf [5], Nedele and Wisnom [6], Landis, Phoenix and Beyerlein [7-9] and Lagoudas [10], there is a fundamental lack of comprehensive experimental evidence to validate the models, contributing to the use of high safety factors and overdesign in composites engineering.

Macroscopic properties and mechanical behaviour stem from micromechanical parameters, including: variability of fibre and matrix strength, interface strengths, local stress concentrations and geometry [11]. As such the nature of damage and its development depends on the microstructure of the material [12]. Damage progression in composites frequently involves a sequential accumulation and interaction of several failure modes (*e.g.* matrix cracks, delaminations and fibre failures), however the exact processes and their interactions are complex and case dependent [13]. The current work focuses on the accumulation and interaction of fibre breaks, a dominant failure mechanism for carbon fibre reinforced materials under tension [14]. Broken fibres of necessity lose their stress-carrying capabilities, transferring load to neighbouring unbroken fibres [15]. Both experimental and modelling work indicate that as damage progresses, individual fibre breaks and clusters of fibre breaks accumulate, with one cluster potentially growing on to cause catastrophic failure

[16]. The size, distribution and number of clusters, along with the fibre ineffective length are all expected to vary with fibre and matrix parameters [17, 18], however explicit, quantitative studies of fibre break accumulation within the volume of engineering composites have only become available very recently (*e.g.* see [14]). The aim of this paper is to illustrate how basic component materials' parameters may influence fibre break density and clustering characteristics for a range of carbon-epoxy composite systems.

2 Methodology

Cross-ply laminate plates were manufactured to a thickness of ~1mm with variety of resin and matrix combinations. Properties for two of the systems are illustrated in Table 1 (both matrices containing toughening phases in this case). The T800/M21 plate provides a direct comparison with previous work [19], where fibre breaks in T700/M21 plates were analysed by the same techniques reported here.

Fibre	Matrix	Fibre UTS (MPa)	Fibre Mod (GPa)	Matrix UTS (MPa)	Matrix Mod (GPa)	Composite UTS (MPa)	Composite Mod (GPa)	Lay-up
T700	M21 [19]	4900	230	23	23	2200	140	$[90/0]_{2s}$
T800	M21	5880	294	23	23	2930	165	$[0_s/90_s]$
IM7	8552	5670	276	121	4.7	2723.1	164.1	$[0_{2s}/90_{2s}]$

Table 1: Composite material properties.

Material properties of the remaining plates are proprietary; however a qualitative overview of the panels is shown in Table 2.

Name	Fibre	Matrix	Lay-up
IMA/T	Intermediate modulus fibre A (IMA)	Toughened	$[90/0]_{2s}$
IMA/UT	Intermediate modulus fibre A (IMA)	Untoughened	
IMB/T	Intermediate modulus fibre B (IMB)	Toughened	
IMB/UT	Intermediate modulus fibre B (IMB)	Untoughened	

Table 2: Overview of composite properties

Specimen preparation and testing methodology follow the procedure laid out by Wright [19]. The plates were cut into 4mm wide double-notched coupons using abrasive water jet cutting; aluminium tabs were bonded to the ends of the coupons to permit loading, and reduce stress concentrations at the coupon ends Fig 1 (a) and (b).

10 coupons of each composite system were initially tensile tested using the *in situ* loading rig shown in Fig 1 (c), to determine the average ultimate tensile strength (UTS) values. Load is applied at the top of the rig through a screw-driven mechanism which causes a linear translation of the upper clevis, transferring a tensile load to the coupon which is restrained by the lower clevis. Belvedere washers make up a compliant section at the top of the rig, ameliorating any time dependent thermal and/or visco-elastic properties of the acrylic tube used for the X-ray imaging 'window'.

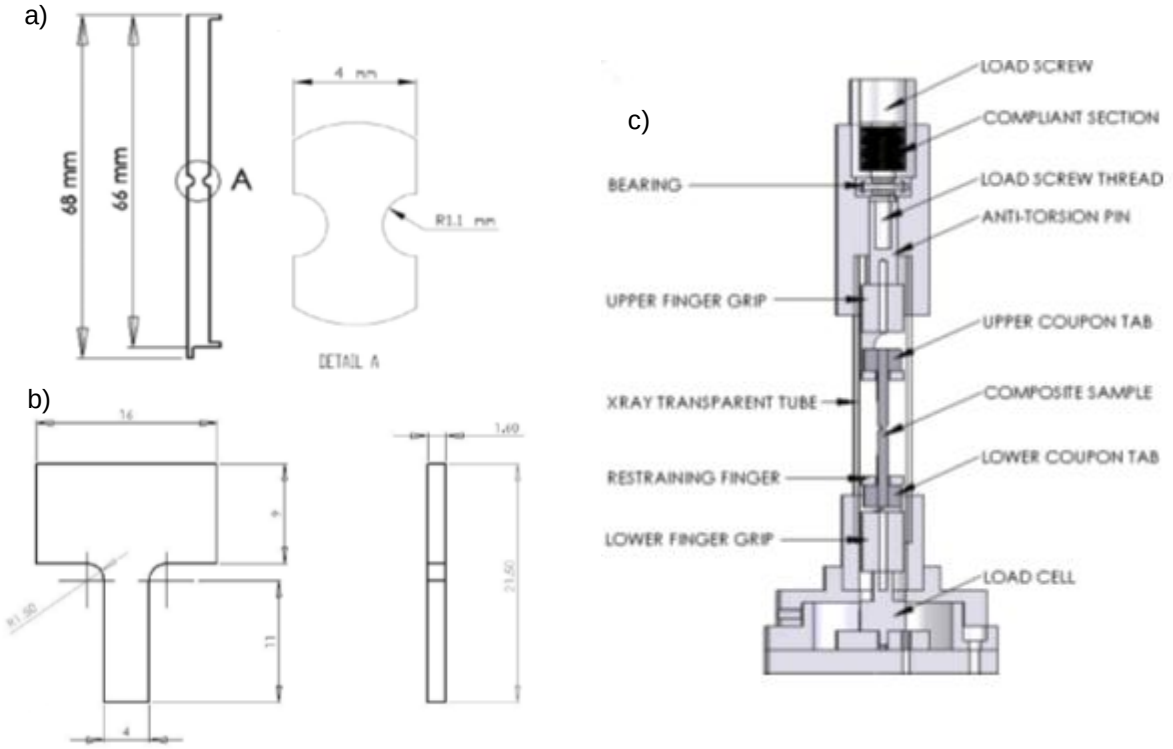

Figure 1. Schematic illustration of: (a) test coupon geometry, (b) aluminium end tab dimensions and (c) loading rig [19].

Coupons of each material were loaded to failure in steps of the order of 10-15% of nominal UTS, with SRCT scans being taken at each step. Whilst applied stress levels on a given coupon could be controlled and recorded to ~1% accuracy, exact loads as a fraction of UTS could not be controlled closely due to the inevitable variability in UTS values for individual samples.

Scans were undertaken on the TOMCAT beamline at the Swiss Light Source (SLS), at an energy of 17kV, with an isotropic voxel resolution of 0.6μm. This setup allows for satisfactory identification of individual fibres and micromechanical damage evolution at scan times of approximately 7 minutes (1501 projections). A sample-detector propagation distance of 30mm was used, producing a degree of near-field Fresnel edge enhancement. Reconstruction was undertaken using in-house software at the SLS. Subsequent image processing and analysis was performed in Volume Graphic VG Studio Max and ImageJ/FIJI. Fibre breaks were identified by visual inspection in three orthogonal planes to ensure that imaging artefacts and other microstructural features were not included in the analysis. An example of a fibre break in two different orthogonal planes is given below, Figure 2.

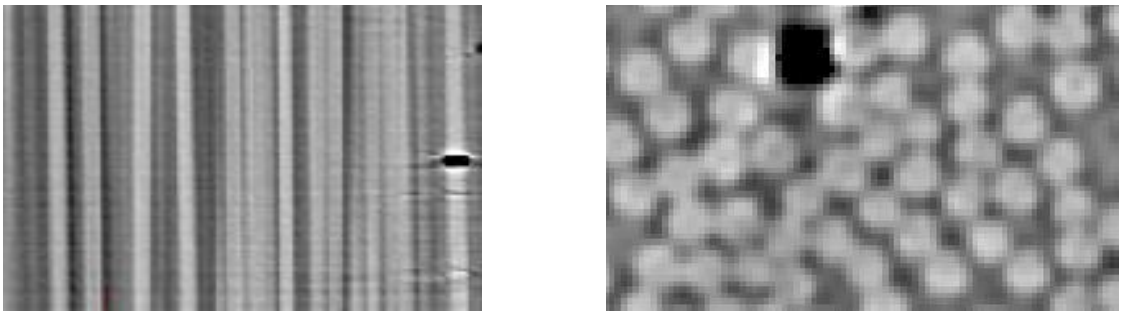

Figure 2. Example fibre break seen parallel and perpendicular to the fibre orientation.

3. Results and Discussion

Variations in exact UTS levels of each sample prevented exact, like-for-like comparison of damage accumulation steps in terms of percentages of UTS level (*i.e.* exact UTS values are only known once a sample is taken to failure). Table 3 shows the highest common percentage increment achieved for the 5 of the 6 system types analysed, *i.e.* ~ 90%, along with the highest percentage of UTS for which a scan was obtained prior to specimen fracture. Scott *et al.* found a significant acceleration of break accumulation from around 80% of UTS in the T700/M21 system (although fibre breaks are also detected well below this level) [14].

	Material					
	T800/M21	IM7/8552	IMA/T	IMA/UT	IMB/T	IMB/UT
Nominal %UTS	80	95	95	80	70	93
Actual %UTS	87	90	92	91	82	93
Highest %UTS imaged	87	95	98	91	82	98

Table 3: Closest common load step achieved in all systems and highest load step reached in each.

It can be seen that for five out of the six specimens, load steps (and hence SRCT scans) were obtained close to 90% of UTS, within a ±3% range. The fibre break densities for each of the conditions indicated in Table 3 were calculated and plotted in Figure 3. Progressive accumulation of fibre breaks with load in T700/M21 reported by Scott *et al.* are also shown. Although only a limited number points from each sample have been obtained to date, it can be seen that two of the materials, IMB/T and T800/M21, fall significantly (factor >2) above the trend for T700/M21, whilst those for IM5/8552 and IMB/UT appear to be of the same order.

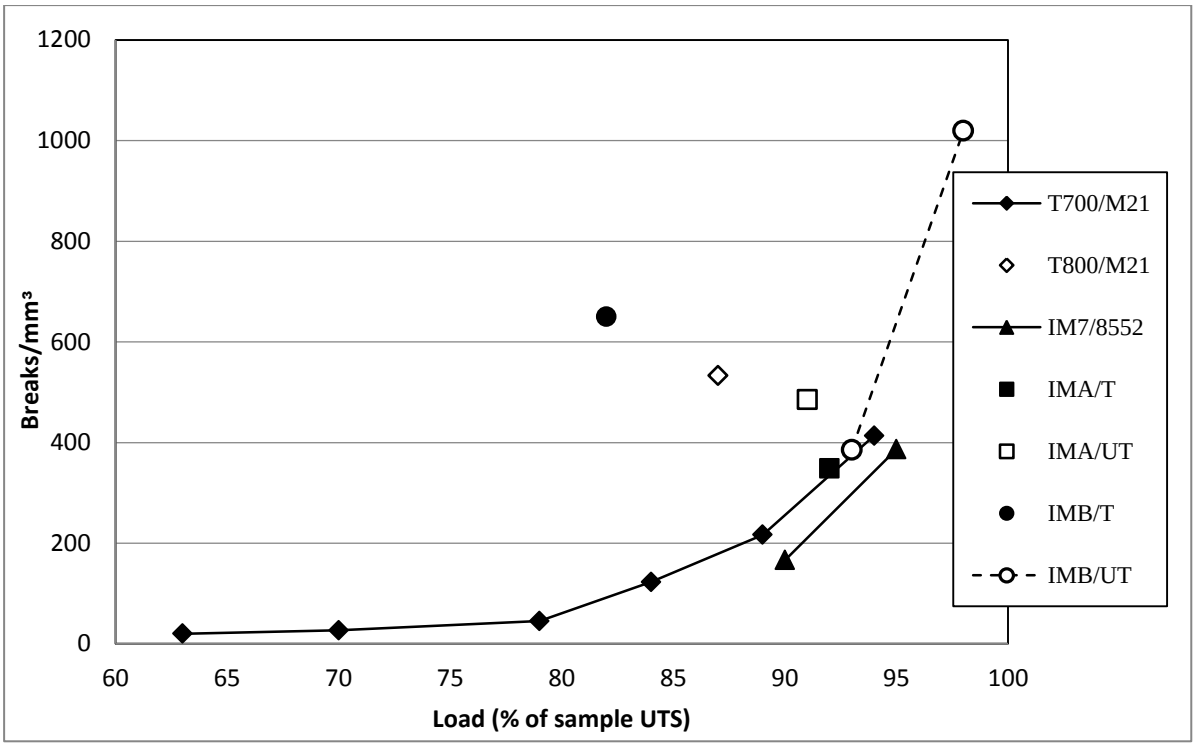

Figure 3: Fibre break accumulation vs. %UTS

The *in situ* loading allows for the damage progression and accumulation of clusters to be monitored and quantified, with Scott *et al.* reporting cluster formations with load for pre-preg plate (as tested here) and filament wound material of the same fibres [24]. For the pre-preg samples analysed at 94%, large clusters (6, 8 and 14 fibre breaks) were reported, whilst for the filament wound material the largest cluster observed was a 4-plet [20]. Scott *et al.* also found that for every singlet in the pre-preg material there were many more clusters (2-plet and higher) when compared with filament wound material. Initial qualitative assessment of current results in terms of breaks in immediately neighbouring fibres revealed large clusters (4-plet and above) in only two of the systems tested IMB/UT (98%UTS) and IM7/8552 (95%UTS). In IMB/UT (98%UTS) three 4-plets, two 5-plets, one 6-plet and one 7-plet were identified; whilst in IM7/8552 a 4-plet and a 6-plet were identified. 2-plets and 3-plets were identified in all samples other than IMA/T.

Scott *et al.* also reported that the geometrical form of break clusters differed. Clusters found in filament wound material frequently occurred with separation in the fibre axis direction: in contrast, clusters in pre-preg material were frequently co-planar, consistent with little or no fibre debonding influence on cluster formation [20]. Examples of clusters in the current systems are shown in Figure 4. Figure 4(a) illustrates a co-planar cluster across multiple fibres. Whilst statistical quantification is ongoing, it was seen that the majority of break clusters in IMB/UT showed clear axial separations, whilst clusters in the other specimens (IM7/8552, T800/M21, IMA/UT) frequently showed co-planar break events.

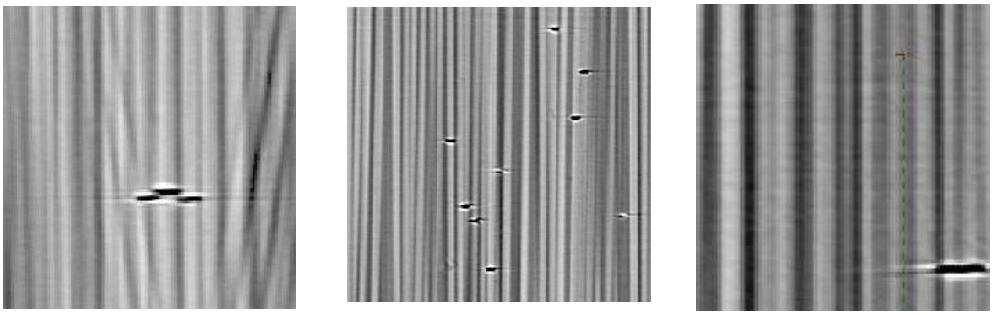

(a) (b) (c)

Figure 4: Break cluster geometries observed in (a) IM7/8552, (b) IMB/UT and (c) IMA/UT

The available data allow for some estimation of the fibre ineffective length (approx. upper bound values), with ineffective lengths of the coupons tested here identified to lie in the range of ~30-90μm across the material types, compared with a previously reported value of 70μm for T700/M21

4 Conclusions

Synchrotron radiation computed tomography has been used to analyse the effects of fibre and matrix types on fibre break densities, fibre break clustering and fibre ineffective lengths. Whilst further statistical and geometrical analysis of other load steps is ongoing, it is identified that:

- The material with the highest break density (IMB/UT) also had the greatest number of large clusters (4-plets and above). This material also showed a reduced propensity for co-planar fibre breaks.
- Apparent ineffective lengths of the materials tested ranged from ~30-90μm.

Acknowledgments

The authors gratefully acknowledge Hexcel and Cytec Industries for materials supply. The authors would also like to acknowledge support of the μ-VIS X-ray Imaging Centre at Southampton (www.southampton.ac.uk/muvis) and the staff at the TOMCAT/SLS beamline.

References

1. Rizzo, P. and F.L. Di Scalea, *Acoustice Emission Monitoring of Carbon-Fibre-Reinfprced-Polymer Bridge Stay Cables in Large-Scale Testing.* Experimental Mechanics, 2001. 41(3).
2. Blassiau, S., A. Thionnet, and A.R. Bunsell, *Micromechanisms of Load Transfer in a Unidirectional Carbon Fibre-Reinforced Epoxy Composite due to Fibre Failures: Part 3. Multi-Scale Reconstruction of Composite Behaviour.* Composite Structures, 2008. 83.
3. Bohse, J., *Acoustic Emission Characteristics of Micro-Failure Processes in Polymer Blends and Composites.* Composites Science and Technology, 2000. 60.
4. Zweben, C. and B.W. Rosen, *A Statistical Theory of Material Strength with Application to Composite Materials.* Journal of the Mechanics and Physics of Solids, 1970. 18: p. 189-206.
5. Batdorf, S.B. and R. Ghaffarian, *Size Effect and Strength Variability of Unidirectional Composites.* International Journal of Fracture, 1984. 26: p. 113-123.
6. Nedele, M.R. and M.R. Wisnom, *Three-Dimensional Finite Element Analysis of the Stress Concentration at a Single Fibre Break.* Composite Science and Technology, 1993. 51: p. 517-524.

7. Beyerlein, I.J. and S.L. Phoenix, *Statistics of Fracture for an Elastic Notched Composite Lamina Containing Weibull Fibres- Part II. Probability Models of Crack Growth.* Engineering Fracture Mechanics, 1997. 57(2/3): p. 267-299.
8. Beyerlein, I.J. and S.L. Phoenix, *Stress Concentrations Around Multiple Fibre Breaks in an Elastic Matrix with Local Yielding or Debonding using Quadratic Influence Superposition.* Journal of Mechanics and Physics of Solids, 1996. 44(12): p. 1997-2039.
9. Landis, C.M., I.J. Beyerlein, and R.M. McMeeking, *Micromechanical Simulation of the Failure of Fibre Reinforced Composites.* Journal of the Mechanics and Physics of Solids, 2000. 48: p. 621-648.
10. Lagoudas, D.C., C.-Y. Hui, and S.L. Phoenix, *Time Evolution of Overstress Profiles near broken Fibres in a Composite with a Viscoelastic Matrix.* International Journal of Solids Structures, 1988. 25(1): p. 45-66.
11. Van de Heuvel, P.W.J., Y.J.W. Van de Bruggen, and T. Peijs, *Failure Phenomena in Multi-Fibre Model Composites: Part 1. An Experimental Investigation into the Influence of Fibre Spacing and Fibre-Matrix Adhesion.* Composites Part A, 1996. 27(A): p. 855-859.
12. Berthelot, J.M. and J. Rhazi, *Acoustic-Emission in Carbon-Fiber Composites.* Composites Science and Technology, 1990. 37(4): p. 411-428.
13. Siron, O. and H. Tsuda, *Acoustic emission in carbon fibre-reinforced plastic materials.* Annales De Chimie-Science Des Materiaux, 2000. 25(7): p. 533-537.
14. Scott, A.E., et al., *Damage Accumulation in a Carbon/Epoxy Composite: Comparison between a Multiscale Model and Computed Tomography Experimental Results.* Composites Part A, 2012.
15. Chen, R.C., et al., *Measurement of the linear attenuation coefficients of breast tissues by synchrotron radiation computed tomography.* Physics in Medicine and Biology, 2010. 55(17): p. 4993-5005.
16. Ibnabdeljalil, M. and W.A. Curtin, *Strength and Reliability of Notched Fibre-Reinforced Composites.* Acta Materialia, 1997. 45(9): p. 3641-3652.
17. Fukuda, H. and K. Kawata, *On the Stress Concentration Factor in Fibrous Composites.* Fibre Science and Technology, 1976. 9: p. 189-203.
18. Fukuda, H., *Stress Concentration Factors in Unidirectional Composites with Random Fibre Spacing.* Composites Science and Technology, 1985. 22: p. 153-163.
19. Wright, P., et al., *Ultra High Resolution Computed Tomography of Damage in Notched Carbone Fibre-Epoxy Compositess.* Journal of Composite Materials, 2008. 42(19): p. 1993-2002.
20. Scott, A., et al., *High Resolution Damage Detection of Loaded Carbon/Epoxy Laminates using Synchrotron Radiation Computed Tomography*, in *18th ICCM*. 2011: Korea.